

86 GHz SiO maser survey of late-type stars in the Inner Galaxy *

II. Infrared photometry of the SiO Target Stars

M. Messineo¹, H. J. Habing¹, K. M. Menten², A. Omont³, and L. O. Sjouwerman⁴

¹ Leiden Observatory, P.O. Box 9513, 2300 RA Leiden, the Netherlands
e-mail: messineo@strw.leidenuniv.nl; habing@strw.leidenuniv.nl

² Max-Planck-Institut für Radioastronomie, Auf dem Hügel 69, D-53121 Bonn, Germany
e-mail: menten@mpifr-bonn.mpg.de

³ Institut d’Astrophysique de Paris, CNRS & Université Paris 6, 98bis Bd Arago, F 75014 Paris, France
e-mail: omont@iap.fr

⁴ National Radio Astronomy Observatory, P.O. Box 0, Socorro NM 87801, USA
e-mail: lsjouwerman@aoc.nrao.edu

Received October 09, 2003; accepted December 19, 2003.

Abstract. We present a compilation and study of DENIS, 2MASS, ISOGAL, MSX and IRAS 1–25 μ m photometry for a sample of 441 late-type stars in the inner Galaxy, which we previously searched for 86 GHz SiO maser emission (Messineo et al. 2002). The comparison of the DENIS and 2MASS J and K_S magnitudes shows that most of the SiO targets are indeed variable stars. The MSX colours and the IRAS [12] – [25] colour of our SiO targets are consistent with those of Mira type stars with dust silicate feature at 9.7 μ m feature in emission, indicating only a moderate mass-loss rate.

Key words. stars: AGB and post-AGB – Infrared: stars – Stars: variables: general – circumstellar matter – masers – Galaxy: stellar content

1. Introduction

Stars of intermediate mass, $1 < M_* < 6 M_\odot$, enter a phase of intense mass loss when they reach the Asymptotic Giant Branch (AGB). As a consequence, they are surrounded with a dense envelope of dust and molecular gas. Due to the low effective temperature and the dust thermal emission, AGB stars are bright at infrared wavelengths and can be detected even towards highly obscured regions. Furthermore, the maser emission from their envelopes is strong enough to be detected throughout the Galaxy, and radio spectroscopic observations can provide the stellar line-of-sight velocities to within a few km s^{-1} (e.g. Habing

1996). AGB stars thus permit a study of Galactic kinematics, structure, and mass-distribution.

To understand the Galactic structure and kinematics it is important to combine the kinematic information and the stellar properties, e.g. luminosities, which can provide a distance estimate. Good photometry on infrared point sources toward the inner Galaxy is now available from large surveys such as DENIS (Epchtein et al. 1994), 2MASS (Cutri et al. 2003), ISOGAL (Omont et al. 2003; Schuller et al. 2003) and MSX (Egan et al. 1999; Price et al. 2001). Since the high extinction toward the inner Galaxy precludes studies at optical wavelengths, these infrared data permit a unique view of its stellar population. The combination of near- and mid-infrared photometry enable us to examine the nature of the stars, i.e. to derive their luminosities, mass-loss rates, and to discriminate against foreground stars.

To improve the line-of-sight velocity statistics, we conducted 86 GHz $v = 1, J = 2 \rightarrow 1$ SiO maser line observations of 441 late-type stars in the inner Galaxy ($30^\circ < l < -4^\circ$, $|b| < 1$) with the IRAM 30-m telescope (Messineo et al. 2002, hereafter Paper I). This paper is part of a series devoted to characterise the properties, i.e. mass-loss rates and luminosities, of the 441 sources previ-

Send offprint requests to: M. Messineo

* This is paper no. 21 in a refereed journal based on data from the ISOGAL project.

Based on observations with ISO, an ESA project with instruments funded by ESA member states and with the participations of ISAS and NASA.

Based on observations collected at the European Southern Observatory, La Silla Chile.

Based on observations carried out with the IRAM 30-m telescope located at Pico Veleta. IRAM is supported by INSU/CNRS (France), MPG (Germany) and IGN (Spain).

ously targeted to search for 86 GHz SiO maser emission (Paper I).

Here (Paper II) we present the available near- and mid-infrared photometry of the targeted sources (“SiO targets” hereafter). In another paper (Messineo et al. 2003a, hereafter Paper III) we deal with extinction correction and finally in the last paper (Messineo et al. 2003b, hereafter Paper IV) we compute and analyse the luminosities of the SiO targets.

The spatial distribution of the 441 targets is shown in Fig. 1. These SiO targets are divided into two subsamples: 253 sources were selected from the ISOGAL catalogue, (“the ISOGAL sample”), and 188 sources from the MSX catalogue, (“the MSX sample”). The ISOGAL and MSX samples are examined to test whether both are drawn from the same “parent population”. Brightness variability is studied by a comparison of the DENIS and 2MASS photometry.

The structure of the paper is as follows: in Sect. 2 we identify our SiO targets in various infrared catalogues and collect their magnitudes finding for many stars up to fourteen different measurements. In Sect. 3 we compare the statistical differences between our ISOGAL and MSX samples. In Sect. 4 we summarise additional information found with SIMBAD, e.g. variability and other types of masers, and we derive the probability of association between the radio maser and the infrared counterpart. The brightness variability of the stars is discussed in Sect. 5. In Sects. 6 and 7 we analyse the mid-infrared colours of the stars and compare them with those of OH/IR stars. The main conclusions are summarised in Sect. 8.

The individual source numbers (e.g. #99) are taken from Table 2 (86 GHz SiO maser detections) and Table 3 (non-detections) in Paper I unless otherwise indicated. The SiO maser emission in this paper generally refers to the 86 GHz ($v = 1, J = 2 \rightarrow 1$) SiO maser only and not to the 43 GHz ($J = 1 - 0$) SiO masers. Velocities in this paper refer to line-of-sight velocities with respect to the Local Standard of Rest.

2. Identification of the SiO targets in various infrared catalogues

We cross identified all SiO targets, whether taken from the ISOGAL or from the MSX database, with all infrared catalogues available to us, the DENIS, 2MASS, ISOGAL, MSX and IRAS survey catalogues. The results are summarised in Table 1. In the following, we briefly recall the criteria used for the selection of the ISOGAL and the MSX samples and describe the modality of the cross-correlations. More details on the selection criteria can be found in Paper I.

2.1. ISOGAL data

ISOGAL (Omont et al. 2003) is a 7 and 15 μm survey taken with ISOCAM (Cesarsky et al. 1996) aboard the Infrared Space Observatory (ISO) satellite (Kessler et al.

1996). The 16 deg^2 survey consists of selected sub-fields along the Galactic plane, mostly concentrating on the Galactic Centre. With a sensitivity approaching 10 mJy (two orders of magnitude deeper than IRAS and one order of magnitude deeper than MSX) and a resolution of 3-6” ISOGAL has detected over 100,000 objects. The ISOCAM data have been correlated with the DENIS near-infrared I , J and K_S band data to produce the five band ISOGAL-DENIS point source catalogue (ID-PSC) (Schuller et al. 2003). The ID-PSC reports the photometric data in magnitudes. The astrometric accuracy of the ID-PSC is determined by the present DENIS astrometric accuracy better than 0.5”.

Sources were selected from a preliminary version of the ISOGAL catalogue by their extinction-corrected 15 μm magnitude, $[15]_0$, and their $(K_{S0} - [15]_0)$ and $([7]_0 - [15]_0)$ colours approximately corrected for extinction (Sect. 7.3.2 Paper I). The brightest 15 μm sources, $[15]_0 < 1.0$, and those with $([7]_0 - [15]_0) < 0.7$ and with $(K_{S0} - [15]_0) < 1.95$ were excluded since they are likely to be foreground stars or non-AGB stars or AGB stars with very small mass-loss. Further, sources with $[15]_0 > 3.4$ were excluded since they are likely to show SiO maser emission fainter than our detection limit of 0.2 Jy. Sources with $([7]_0 - [15]_0) > 2.3$ were excluded since they are likely to be compact HII regions or other young stellar objects or planetary nebulae. Those with $(K_{S0} - [15]_0) > 4.85$ were excluded because they are likely to be OH/IR stars with a high mass-loss rate or young stellar objects. Moreover, known OH/IR stars were discarded as the kinematic data are already known.

2.2. MSX data

The Midcourse Space Experiment (MSX) is a survey at five mid-IR bands ranging from 4.3 μm [$B1$ band] to 21.4 μm [E band], with a sensitivity of 0.1 Jy in A band (8.28 μm) and a spatial resolution of 18.3” (Price et al. 2001). The survey covers the Galactic plane to $\pm 5^\circ$ latitude. Version 1.2 of the MSX-PSC (Egan et al. 1999) lists more than 300,000 point sources with an rms astrometric accuracy of $\sim 2''$. The MSX catalogue gives the source flux density, F , in Jy. Magnitudes are obtained adopting the following zero-points: 58.49 Jy in A (8.26 μm) band, 26.51 Jy in C (12.12 μm) band, 18.29 Jy in D (14.65 μm) band and 8.80 Jy in E (21.41 μm) band (Egan et al. 1999).

For the MSX source selection we used flux densities in the A and D bands which have wavelength ranges roughly similar to the ISOGAL 7 and 15 μm bands. We selected those non-confused, good-quality sources in A and D band (flag > 3), which show variability in the A band. We avoided the reddest stars, $F_D/F_A > 2.3$ ($A - D > 2.2$ mag). We also avoided the bluest and most luminous stars with $F_D/F_A < 0.6$ ($A - D < 0.75$ mag) and $F_D > 6$ Jy ($D < 1.2$ mag) since they are likely to be foreground stars or supergiants (Schuller 2002; Schultheis et al. 2003). Furthermore, following the classi-

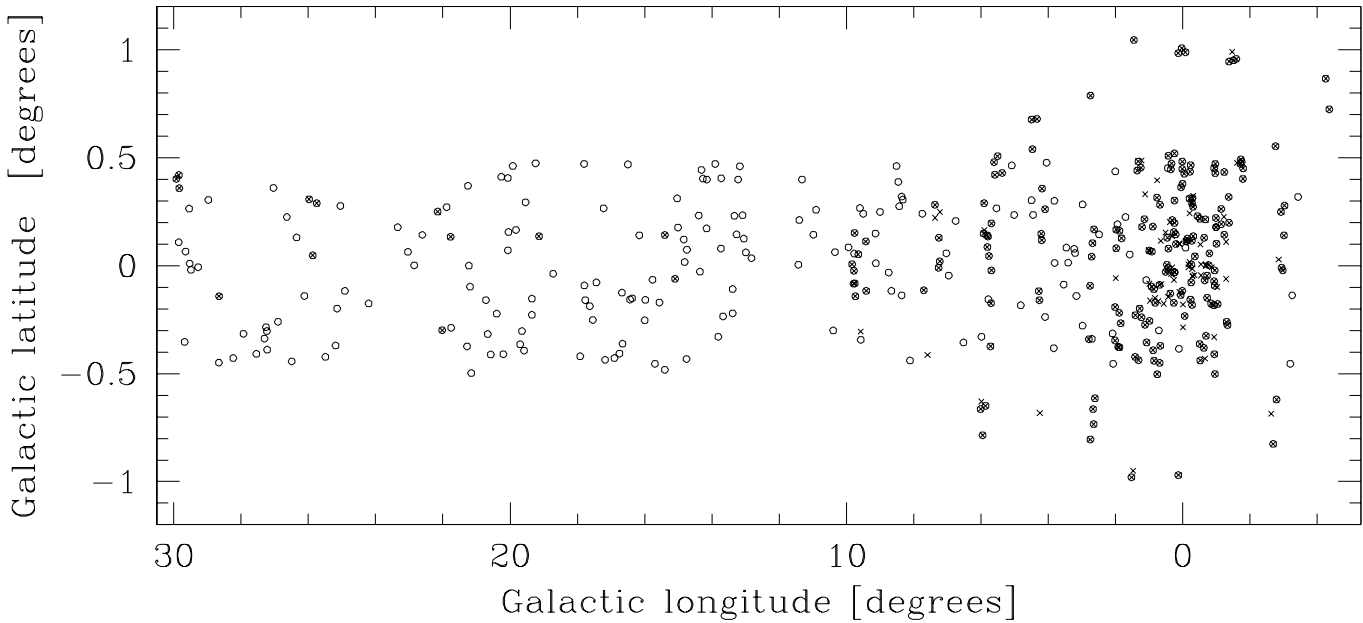


Fig. 1. Location of the 441 SiO targets in Galactic coordinates. The 379 MSX counterparts are shown as open circles, the 267 ISOGAL counterparts as crosses. Overlap of MSX and ISOGAL sources resemble filled symbols. Four points fall outside the figure.

Table 1. Number of counterparts of our SiO targets

	2MASS			DENIS			ISOGAL			MSX		IRAS	
	all sky data release			bulge PSC			PSC 1.0			PSC 1.2		PSC 2.0	
	J	H	K _S	I	J	K _S	(Cutri et al. 2003)	(Simon 2003)	(Schuller et al. 2003)	(Egan et al. 1999)	(Beichman et al. 1988)		
ISO (253)	252	252	252	53	217	253			253	191		43	
MSX (188)	187	187	187	42	149	188			14	188		122	
Total (441)	+439	++439	439	95	*366	**441			267	379		165	

+ 72 are upper limits * 16 have magnitudes above saturation limits

++ 13 are upper limits ** 104 have magnitudes above saturation limits

fication of Kwok et al. (1997) of IRAS sources with low-resolution spectra, we used the C to E band ratio to discard very red ($F_E/F_C > 1.4$, $C - E > 1.55$ mag) sources, which are likely to be young stellar objects or OH/IR stars with thick envelopes. Known OH/IR stars were excluded.

2.3. ISOGAL-MSX cross-identifications

More than half (253) of our sample of SiO targets were selected from the ISOGAL survey, indeed from a preliminary version of the ID-PSC (Paper I). They are all in an area covered by the MSX survey. For each of our 253 ID-PSC selected SiO targets we searched for the closest associated source in the MSX-PSC within $15''$ from the SiO target position. We found counterparts for 191 of them, 190 of which were unique. The distribution of the angular separations is shown in Fig. 2; the mean and median angular separation are $3.3''$ and $3.0''$ with a standard deviation of $2.1''$, the maximum separation is $10.4''$. To estimate the likely number of chance associations, we re-

peated the cross-correlation after shifting all ID-PSC positions between $30''$ and $100''$ finding that the probability of spurious associations within $11''$ is less than 1%. The 62 ISOGAL sources without a counterpart in the MSX-PSC are mostly (55) concentrated in the central 3 degrees from the Galactic Centre. Their $7\ \mu\text{m}$ ISOGAL fluxes range from 0.4 Jy to 1.5 Jy, whereas for the 191 associated sources, the flux is on average 1.6 Jy with a standard deviation of 1.3 Jy. Thus, the ISOGAL/non-MSX sources are likely to have been excluded from the MSX-PSC because of confusion due to the high stellar density in the inner Galaxy. The fraction of our ISOGAL stars without MSX identifications is $\sim 11\%$ for those with $7\ \mu\text{m}$ magnitude $[7] < 4.5$ ($F_7 > 1.3$ Jy).

Out of the 188 SiO targets selected from the MSX catalogue, only 14 are located in an ISOGAL field, and we found ID-PSC identifications for all of those within $5''$ from the MSX positions. For the remaining 174 sources we searched the DENIS PSC.

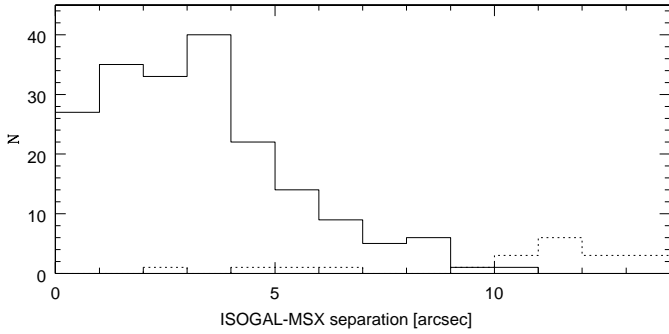


Fig. 2. Associations between our SiO ISOGAL targets and the MSX catalogues. The distribution of the angular separations (''') between the ISOGAL and the MSX positions (continuum line). For comparison, the dashed line is the total distribution of the chance associations, found by performing five shifting experiments.

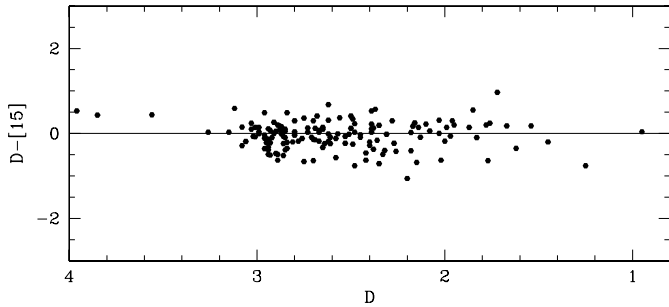


Fig. 3. Difference between the MSX band D magnitude, D , and the ISOCAM 15 μm magnitudes, [15], versus the D . Magnitude zero point in D band was taken from Egan et al. (1999). The continuous line is $D - [15] = 0.0$ mag

As the ISOCAM 15 μm and MSX D filters are similar, we compared the ISOCAM 15 μm magnitudes, [15], and the MSX D band magnitudes, D , of the 154 sources detected at 15 μm in both surveys and found good agreement (Fig. 3); the average difference $D - [15]$ is -0.04 magnitude and the standard deviation is 0.3 mag, resulting from the combination (~ 0.15 mag) of the photometric errors of both catalogues and from the possible intrinsic source variability.

2.4. DENIS data

DENIS is a simultaneous I (0.8 μm), J (1.25 μm), and K_S (2.15 μm) band survey of the southern hemisphere using the ESO 1-meter telescope at La Silla (Epcstein et al. 1994). The 3σ detection limit in the respective bands is 0.05 mJy (19 mag), 0.5 mJy (16 mag) and 2.5 mJy (13.5 mag), and the saturation limit is at magnitudes 10, 7.5 and 6, respectively. The absolute DENIS astrometry is fixed using the USNO-A2.0 catalogue. The current absolute astrometric accuracy of DENIS is better than 0.5'' (rms) (see Sect. 4.2 in Schuller et al. 2003).

2.4.1. ISOGAL sample and DENIS identifications

For the SiO targets selected from the ISOGAL survey, a proper DENIS identification and photometry had already been provided (Schuller et al. 2003; Simon 2003). For each ISOGAL field, a sample of DENIS point sources from the same area was extracted. DENIS coordinates were retained as the astrometric reference system and a polynomial distortion correction was applied to the ISOGAL coordinates in order to match as best as possible the ISOGAL and DENIS reference coordinates. In order to reduce the number of spurious associations, only DENIS sources with a K_S detection were selected and a K_S upper limit was imposed according to field density (Schuller et al. 2003). Among our 253 ISOGAL targets all have a DENIS K_S identification, while only 86% and 21% have J and I detections, respectively.

2.4.2. MSX sample and DENIS identifications

We searched for possible DENIS counterparts to the 188 SiO targets which we had selected from the MSX catalogue. For all sources from the MSX sample we searched the provisional bulge DENIS PSC (Schuller et al. 2003; Simon 2003) for the nearest K_S band object. As late-type stars are intrinsically red, only K_S band counterparts were examined. As saturated sources are usually given in the catalogue with null magnitude, DENIS photometry from other observations (Epcstein et al. 1994) and the K_S images were used as additional checks for saturated counterparts to the MSX SiO targets. Fortunately, such DENIS data was available for all MSX sources that we observed; however, a large number of bright sources saturated the detector in the K_S band. While all sources were detected in the K_S band, the fraction of detections in the J and I band was 79% and 22%, respectively.

The distribution of angular separations of the K_S band counterparts identified is shown in Fig. 4. The mean and median separations are 3.0'' and 2.7'' with a standard deviation of 1.8'', respectively, which is consistent with the expected scatter due to positional uncertainties for the MSX and DENIS catalogues.

To find the distribution of random chance associations we again searched the nearest neighbours after shifting the coordinates of the SiO targets by 30''. The resulting distribution of separations and magnitudes is also shown in Fig. 4. The real associations are on average much brighter and closer than the chance associations. To compute the expected number of incorrect identifications we divided the "chance" distribution in magnitude bins, $(m, m + \Delta m)$, and in each bin computed the normalised cumulative chance distribution of the separations, $f(m, r)$, i.e., the fraction of all chance associations with those magnitudes and within a radius r . We then computed the sum $\Sigma f(m, r)$ over all "real" associations, each being characterised by m and r . Thus, $f(m, r)$ gives the probability for an association to be spurious, and the sum over all sources yields the total expected number of spurious identifica-

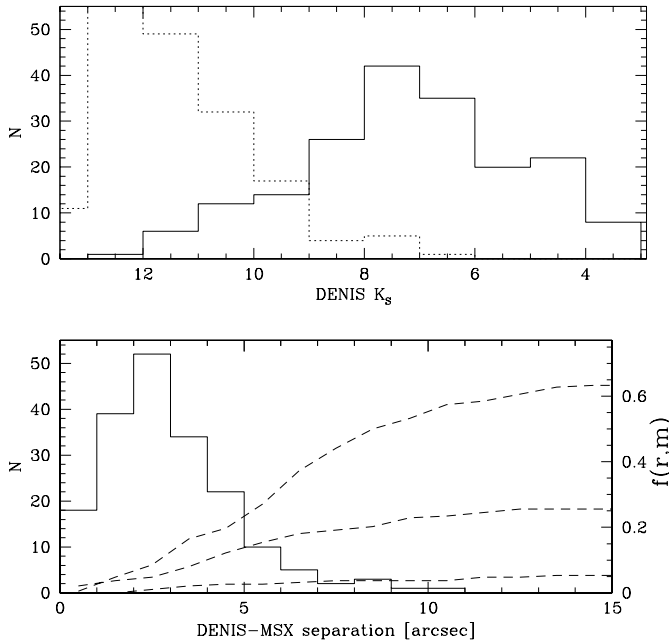


Fig. 4. Associations of our SiO MSX targets in the DENIS catalogue. **Top panel:** distribution of K_s magnitudes for the associations (continuum line) and for the chance associations (dashed line). **Lower panel:** The continuous line shows the distribution of angular separations. The dashed lines show the normalised cumulative distributions, $f(r, m)$, of chance associations found by misaligning the catalogue and MSX SiO targets, where we plot separately, starting from the bottom, the distributions of sources with $K_s < 9$, $9 < K_s < 11$, and $K_s > 11$ mag, respectively.

tions. When we consider only the brightest identifications for the 154 sources with a $K_s < 9$ mag counterpart, only two spurious identifications are expected. For the 34 possible identifications with $K_s > 9$ mag, we would expect three to be spurious. In total, we expect that about five of our identifications may be incorrect.

Since for the fainter possible counterparts the chance of a false identification is higher, we looked for brighter possible identifications somewhat further away, which due to the lower surface density of brighter sources might have a higher probability to be the actual counterpart. In a few cases (#231, #243, #367, #405, #406, and #424) we found brighter sources somewhat further away but with a lower value of $f(m, r)$ than the closest identification. This suggested that these brighter sources were more likely to be the correct counterparts, which we therefore retained. For these MSX targets with dubious near-infrared association, we additionally examined other MSX sources in their surrounding and checked for possible astrometric shifts between the DENIS and MSX coordinates which could uniquely identify the correct near-infrared counterpart. However, because of the low MSX source density (~ 1 source per $4' \times 4'$), only few associations could be confirmed in this way. Seven sources

could only be associated with a $K_s > 11$ mag counterpart (#162, #273, #363, #403, #417, #423, #443) within $15''$ (beam size of the IRAM telescope).

2.5. 2MASS data

The Two Micron All Sky Survey (2MASS) has surveyed the entire sky at near-infrared wavelengths from the Whipple Observatory on Mt. Hopkins, AZ, and the Cerro Tololo InterAmerican Observatory (CTIO). The cameras observed simultaneously in the J ($1.25 \mu\text{m}$), H ($1.65 \mu\text{m}$) and K_s ($2.17 \mu\text{m}$) bands with a 10σ sensitivity limit in uncrowded fields of 15.8, 15.1 and 14.3 mag, respectively (Beichman et al. 1998; Cutri et al. 2003). The absolute astrometry has typical uncertainty of $0.1''$ (rms) and is based on the Tycho-2 and UCACr10 catalogue (a new version of the USNO's ACT catalogue). The on-line 2MASS PSC (all sky data release) is accessible at the Infrared Processing and Analysis Center (IPAC). 2MASS data was available for all our positions. We retrieved 2MASS sources for our 441 SiO target positions and we searched for the closest positional match. Since the astrometric accuracy is better than $0.5''$ for the ISOGL targets but only $\sim 2''$ for the MSX targets, a different distribution of angular separations is expected for the MSX-2MASS and ISOGL-2MASS associations.

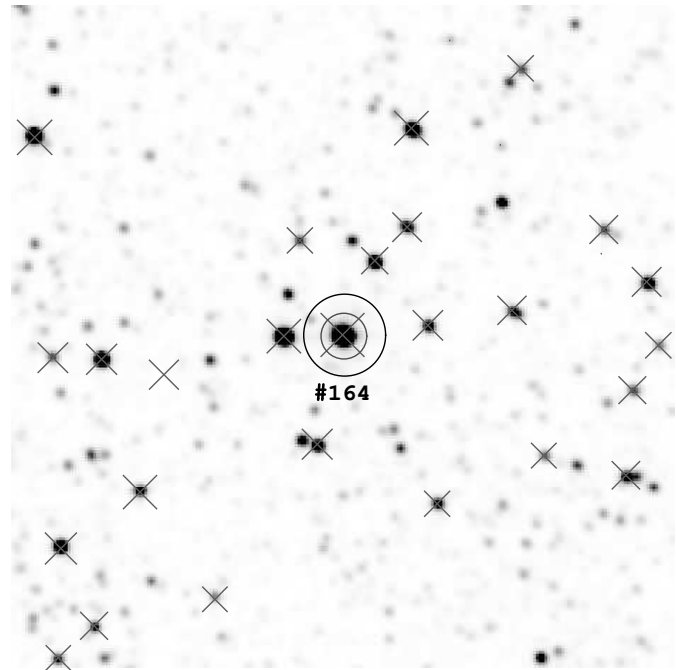


Fig. 5. 2MASS K_s image $230'' \times 230''$ centred at the position of #164. The black circle delimits the main beam (FWHM) of the IRAM telescope used for the SiO maser search. A small gray circle marks the 2MASS association and finally crosses mark sources detected by ISOGL. In agreement with the discussion in the text, all the ISOGL and 2MASS positions are in excellent agreement. Note that the targeted source is the only mid-infrared source falling inside the IRAM telescope beam.

To avoid misidentification, because of the high source density of the 2MASS survey and because the DENIS counterparts are mostly brighter than 11 mag in K_S , we limited the 2MASS K_S magnitude to $K_S < 11$. However, seven sources in our sample, #162, #273, #363, #403, #413, #421 and #423, could be associated only with 2MASS sources fainter than $K_S = 11$ (those sources are also faint in DENIS) within $15''$, which is the beam size of the IRAM telescope. Positional associations were confirmed via overplotting the 2MASS counterpart image with both the SiO targets and the DENIS sources. Finding charts were obtained for all the stars with 2MASS images, an example of which is given in Fig. 5. We found 439 2MASS counterparts and missed only two. In fact, after image inspections, the potential 2MASS counterparts for two sources, #224 and #298, were eliminated as their positions on the 2MASS images were marked by artifacts.

2.5.1. ISOGAL sample and 2MASS identifications

The mean, median separations between the ISOGAL SiO targets (positions as in Paper I, without rounding RA to one tenth of second) and the 2MASS associations are $0.7''$ and $0.3''$ with a standard deviation of $1.0''$, (see Fig. 6).

There is a non-Gaussian tail at large separations. We have individually checked all the sources with separation larger than $3''$ and note that they all have $K_S < 6$. We attribute the large separation to saturation of the DENIS detector. Saturated pixels are an obstacle to the correct determination of the source centroid and this affects the astrometry of saturated stars. Furthermore, most of these bright sources do not have any I associations and therefore the J/K_S astrometry is kept. The mean, median and standard deviation of the separations between the ISOGAL SiO targets and the 2MASS associations with $K_S > 6.5$ mag are $0.4''$, $0.3''$ and $0.4''$; while for 2MASS associations with $K_S < 6.5$ mag they are $1.9''$, $2.1''$ and $1.5''$.

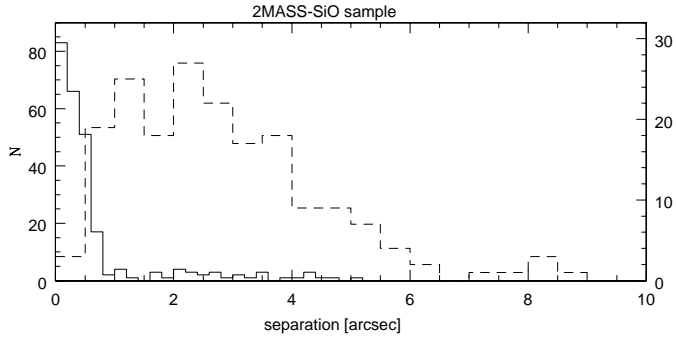


Fig. 6. Distribution of the angular separations between the SiO targets (positions as in Paper I) and the 2MASS associations. The continuum line shows the distribution of the ISOGAL SiO targets and the corresponding y-axis is on the left side. The dashed line shows the distribution of the MSX SiO targets and the relative y-axis is on the right side.

2.5.2. MSX sample and 2MASS identifications

We found 187 2MASS counterparts of MSX SiO targets. The mean, median and standard deviations of the separations between the MSX SiO targets (using the MSX coordinates) and the 2MASS associations are $2.9''$, $2.6''$ and $1.8''$, the same as the separations between the MSX SiO targets and the DENIS associations (see Sect. 2.4.2). This is again consistent with the expected scatter due to positional uncertainties of sources in the MSX and 2MASS catalogues. The mean, median and standard deviation of the separations between the MSX SiO targets (using the DENIS coordinates) and the 2MASS associations are $0.6''$, $0.4''$ and $0.7''$, respectively. The mean, median and standard deviation of the separations in right ascension RA are $0.0''$, $0.0''$ and $0.5''$; while the mean, median and standard deviation of the separations in declination DEC are $-0.2''$, $-0.1''$ and $0.6''$.

2.6. SiO targets and IRAS identifications

We checked for counterparts to our SiO targets in the Infrared Astronomical Satellite Point Source Catalogue (IRAS PSC). Toward the galactic plane the IRAS survey is strongly limited by confusion at the low resolution of the IRAS instruments ($0.5'$ at $12\mu\text{m}$), especially in the longer wavelength bands. Since much of the past work on maser surveys of late-type stars is based on the IRAS data, it may be useful to have an according comparison.

We selected only the 165 IRAS associations within 3.5σ error ellipse of the IRAS PSC, to reduce the chances of spurious associations to $\sim 2\%$ (3 sources). A comparison of $12\mu\text{m}$ fluxes of the prospective counterparts with the ISOGAL and MSX fluxes (Fig. 8) shows a good agreement, confirming that the IRAS identifications are proper. About 35% of our SiO targets have counterparts in the IRAS PSC: 65% of the MSX sample and 17% of the ISOGAL sample. Of those, 96% are detected at $12\mu\text{m}$, 87% at $25\mu\text{m}$, 6% at $60\mu\text{m}$ and 4% at $100\mu\text{m}$, and 56% are reported in the IRAS catalogue as variables (flag > 80).

2.7. SiO targets and visual identifications

Within a radius of $5''$ to our SiO targets we searched for possible visual counterparts in the Tycho 2 and USNO-A2.0 catalogues. We found possible associations for 85 SiO targets, of which 27 are validated by corresponding I band counterparts. Their R magnitudes range from 10.9 to 17.9 and B magnitudes from 13.4 to 20.6. Considering that the pulsation amplitude of Mira stars increases at shorter wavelengths and can be up to 8 mag in the visual (Smak 1964), all those visual stars are possible counterparts of our SiO targets. Most of them are located at latitude $|b| < 0.8^\circ$, but the extinction value inferred by their colours are much smaller than the median of their surrounding stars (Paper III). Therefore they are likely to be foreground stars. Two SiO targets, #7 with $(l, b, vel) = (-1.50^\circ, 0.95^\circ, 18.9 \text{ km s}^{-1})$ and #139 with

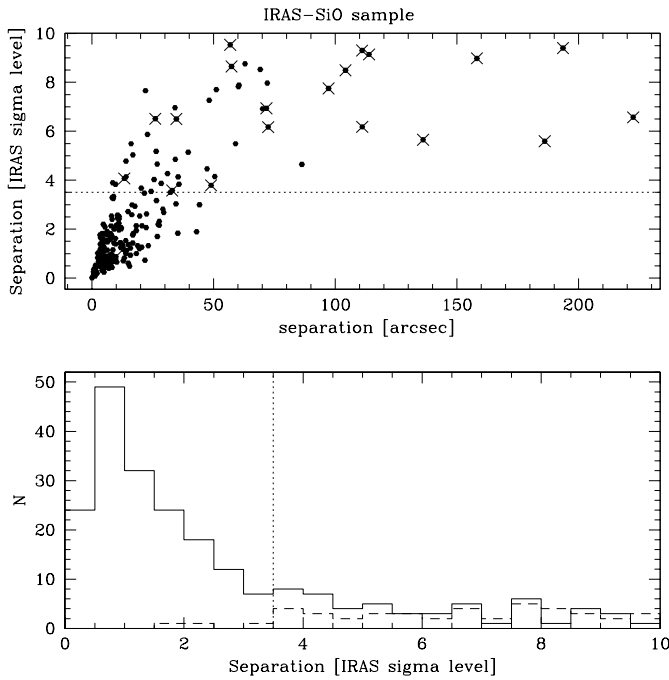


Fig. 7. **Upper panel:** Separation of the possible IRAS counterparts, expressed in IRAS sigma units, against angular separation. Crosses indicate IRAS sources with possible MSX counterparts closer than those associated with the SiO targets; these are likely to be unrelated to the SiO targets. The dotted horizontal line is the upper limit that is selected. **Lower panel:** The continuum line shows the distribution of the separations (in sigma units) of the possible IRAS counterparts. The dashed line shows the distribution of the chance associations obtained shifting the source coordinates by $250''$. The dotted vertical line is our chosen upper limit of 3.5σ .

$(l, b, vel) = (0.31^\circ, -2.18^\circ, 205.7 \text{ km s}^{-1}$), have extinction value inferred by their colours $A_V = 5.5$ and 3 mag, respectively, consistent with the median extinction of their surrounding stars (Paper III). Furthermore, the velocity of #139 is inconsistent with being a foreground star. Therefore we conclude that they are likely located in the Galactic bulge, in regions of low interstellar extinction. In fact, #139 is located in the optical window $W0.2 - 2.1$ at $(l, b) = (0.2^\circ, -2.15^\circ)$ (Dutra et al. 2002; Stanek 1998), and #7 has an extinction value typical of bulge ISOGAL fields with $b \sim +1^\circ$ (Ojha et al. 2003).

2.8. The table

Table 2 lists the infrared photometry of the SiO targets. The columns of Table 2 are as follows: an identification number (*ID*), the same as in Table 2 and 3 of Paper I, followed by the Right Ascension (*RA*), and Declination (*DEC*), in J2000 of the 2MASS counterpart; the DENIS (*I, J, K_S*) magnitudes, the ISOGAL ([7], [15]) magnitudes, the 2MASS (*J, H, K_S*) magnitudes; the angular separation (*dis*), between the adopted near-infrared position and

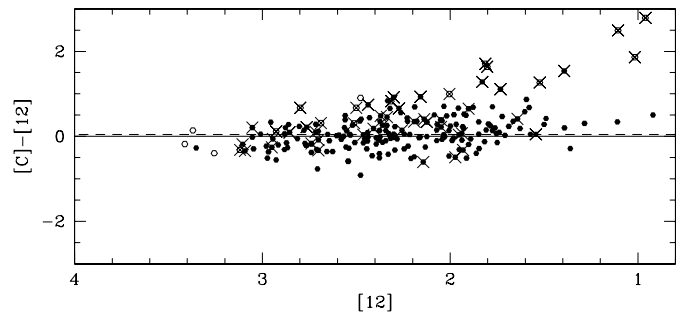


Fig. 8. Difference between the MSX magnitude in the C band, and the IRAS $12\mu\text{m}$ magnitudes, $[12]$, (filled circles) versus the $[12]$. The 18 open circles indicate sources without C measurement, for which the $15\mu\text{m}$ ISOGAL measurement is plotted. Crosses are likely spurious MSX-IRAS associations (angular separation larger than 3.5σ). The plotted IRAS magnitudes are $-2.5 \log(F[\text{Jy}]/28.3)$. The continuous line is $C - [12] = 0.00$ mag and the dashed line is $C - [12] = 0.05$ mag, which is the mean $C - [12]$ colour.

the MSX position, the MSX (*A, C, D, E*) magnitudes, the IRAS 12 and $25\mu\text{m}$ magnitudes and finally a variability flag (*var*), defined as described in Sect. 5. An additional column is used for comments on individual stars.

3. A comparison between the ISOGAL and MSX samples

A large variety of names exists to indicate oxygen-rich AGB stars characterized by different pulsation properties and/or mass-loss rate: semi-regular (SR) stars and Mira stars ($H\alpha$ in emission, visual pulsation amplitude larger than 2.5 mag), large amplitude variables (LAV), long period variable (LPV) stars (when their periods are longer than 100 days), and OH/IR stars (with 1612MHz OH maser emission). In the IRAS colour-colour diagram the oxygen-rich AGB stars are distributed on a well-defined sequence of increasing shell opacity and stellar mass-loss rate (e.g. Habing 1996), which goes from SRs and Miras with the bluest late-type colours and the $9.7\mu\text{m}$ silicate feature in emission, to the coldest OH/IR stars with the reddest colours and the $9.7\mu\text{m}$ silicate feature in absorption. The sequence of increasing shell opacity corresponds also to an increasing $K_S - [15]$ or $K_S - [12]$ colour (e.g. Ojha et al. 2003; Olivier et al. 2001; Whitelock et al. 1994, PaperI).

SiO maser emission is generated in the envelopes of mass-losing AGB stars, close to their stellar photospheres and it occurs more frequently towards oxygen-rich Mira stars than towards other AGB stars (including SR and OH/IR stars) (Bujarrabal 1994; Nyman et al. 1993). Therefore, for our 86 GHz SiO maser survey we selected the brightest sources at $15\mu\text{m}$ with colours of Mira-like stars (PaperI). The ISOGAL and MSX samples were se-

Table 2. Infrared counterparts of the SiO targets.* The identification numbers are the same as in Table 2 and Table 3 of Paper I.

ID	RA(J2000)	DEC(J2000)	DENIS-ISOGAL					2MASS			MSX				IRAS			Comments	
			I	J	K	[7]	[15]	J	H	K	dis	A	C	D	E	[12]	[25]	var	
			[hh mm ss]	[deg mm ss]	[mag]	[mag]	[mag]	[mag]	[mag]	[mag]	''	[mag]	[mag]	[mag]	[mag]	[mag]	[mag]		
1	17 31 40.98	-32 03 55.9	18.29	12.77	8.28	5.16	3.48	12.53	9.66	8.10	3.6	5.40						1	M6, possible visual counterpart no I band association
2	17 36 42.18	-30 59 11.7		14.92	8.16	4.89	3.06	14.67	10.42	8.09	1.0	3.82	2.60	2.35	1.17	2.97	1.58	0	
3	17 37 07.29	-31 21 31.3		12.22	7.53	4.99	3.55	12.42	9.30	7.60	2.5	4.74						2	
4	17 37 29.35	-31 17 16.6		15.01	7.97	4.31	3.44	15.41	10.59	8.08	3.6	4.94	3.25	2.93				2	
5	17 38 11.78	-31 46 27.0		11.78	7.02			11.62	8.70	7.02	4.5	3.36	2.36	2.19	1.25	2.51	1.56	2	
6	17 38 12.49	-29 39 38.5		17.36	11.77	8.06	5.26	2.89	11.73	9.69	8.29							1	
7	17 38 17.07	-29 42 32.4		12.65		6.42	4.63	3.02	7.75	6.22	5.38	1.8	3.92	3.18	2.92		2.44	1.57	2
8	17 38 29.01	-31 26 17.5			10.68	6.85	4.04	2.93	11.01	7.94	6.29	3.5	4.35	3.04	2.86		2.80	0.95	2
9	17 38 32.50	-31 20 42.7			13.94	7.67	4.74	3.44	14.14	9.99	7.75						1.80	0.55	2
10	17 38 35.69	-29 36 37.2		19.15	11.21	7.33	4.59		12.58	9.80	8.12	1.5	3.76	2.76	2.57	1.34	2.81	1.30	2
11	17 39 37.28	-30 08 51.6		16.94	9.99	6.63	4.57	3.09	10.02	7.90	6.67	3.3	4.27	3.14	3.02		2.86	0.69	2
12	17 40 57.23	-29 45 31.4			11.60	7.16	4.07	2.70	11.87	8.87	7.48	2.4	4.32		2.58				2
13	17 41 16.81	-31 38 10.6			13.54	8.30	4.98	3.05	14.04	10.49	8.43	2.2	3.98	2.75	2.42		2.98	1.33	1
14	17 41 26.93	-29 30 47.0			11.80	7.39	4.48	3.56	12.00	9.17	7.39	1.2	5.13						2
15	17 41 31.31	-30 00 18.9		16.43	8.61	6.36	3.24	2.03	7.73	5.73	4.64	4.3	3.09	1.99	1.97	1.04	1.95	0.23	1
16	17 41 36.86	-29 29 31.0			12.23	7.06	3.79	2.00	12.69	9.53	7.58	2.8	3.43	2.43	2.14	1.02			2
17	17 41 37.41	-29 32 05.7			12.26	7.37	4.60	2.85	12.18	9.08	7.30	0.9	4.52		2.61				2
18	17 42 04.36	-29 58 46.4			12.16	7.33	4.83	3.40	13.12	9.88	8.06								2
19	17 42 06.86	-28 18 32.4		15.86	9.59	6.87	4.82	3.12	9.64	7.89	6.88	0.8	4.66	3.57	3.56	3.20			2
20	17 42 23.28	-29 39 35.6			12.52	7.60	5.11	2.95	12.13	9.13	7.46	2.3	4.49	3.12	2.99				2
21	17 42 32.91	-29 41 25.1		17.23	11.78	7.79		4.64	11.62	9.15	7.76								2
22	17 42 32.48	-29 41 10.7			11.94	7.19	4.33	3.08	12.55	9.46	7.67	2.2	4.57	2.93	2.95				2
23	17 42 44.87	-30 04 08.1		16.27	8.65	6.40	4.29	2.71	9.10	6.87	5.67								2
24	17 43 09.81	-29 24 03.3			14.50	7.53	3.65	1.93	15.54	10.79	8.19	3.2	3.43	2.20	1.83	0.90			2
25	17 43 23.46	-28 53 50.3		15.73	8.01	5.99	2.87	2.16	8.44	6.21	4.97	2.5	3.14	2.42	2.18				1
26	17 43 25.26	-29 45 28.6			15.23	8.99	4.92	2.76	15.88	11.69	9.09	2.5	4.29	2.75	2.53				2
27	17 43 32.72	-29 15 39.4			12.06	6.91	3.94	2.45	13.34	9.63	7.47	3.6	3.67	2.72	2.48	1.31			2
28	17 43 33.13	-29 51 33.1			15.00	8.41	4.68	2.88	15.02	10.83	8.42						1.02	0.10	1
29	17 43 34.79	-29 40 30.4				9.15	4.65	2.96	16.90	13.15	9.76								1
30	17 43 35.12	-29 24 47.2				8.82	4.97	2.95	18.47	12.22	9.09	4.0	4.79	2.87	2.85				1

* The full table is available in electronic form at the CDS via anonymous ftp to cdsarc.u-strasbg.fr (130.79.128.5) or via [http://cdsweb.u-strasbg.fr/cgi-bin/qcat?J/A+\(vol\)/\(page\).](http://cdsweb.u-strasbg.fr/cgi-bin/qcat?J/A+(vol)/(page).)

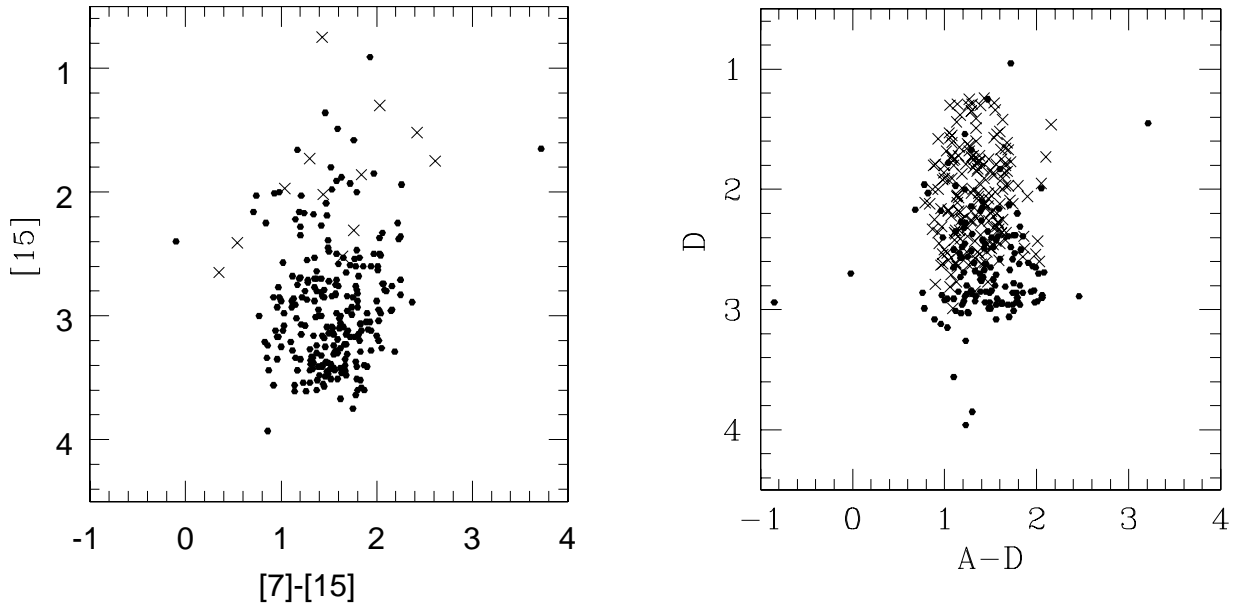


Fig. 9. Mid-infrared colour-magnitude diagrams. **Left-hand panel:** all data from ISOGAL. **Right-hand panel:** all data from MSX. Filled circles indicate targets from the ISOGAL sample and crosses indicate targets from the MSX sample. The two samples have similar mid-infrared colours, due to selection criteria. The numbers of MSX and ISOGAL targets between the two panels vary as explained in Sect. 2.3

lected to have similar 7 and 15 μm colours, as shown in Fig. 9. For the ISOGAL sample a range of intrinsic ($K_S-[15]$)-colour was selected (see Sect. 2.1), but for the MSX sample no near-infrared counterparts were available at the time of the observations, and thus no K_S magnitudes. As an alternative to the ($K_S-[15]$) criterion, for the MSX sample we imposed an upper limit to the ratio of the fluxes in the E (21 μm) and C (12 μm) bands ($C-E < 1.55$ mag). Both criteria were defined in order to avoid non-variable objects and thick envelope objects, but these criteria are not equivalent. The emission in the K_S band is dominated by the stellar emission attenuated by the circumstellar absorption, while circumstellar dust emission contributes strongly to the mid-infrared radiation.

AGB stars with thin envelopes have $C-E < \sim 1.5$ mag, while sources with $C-E > \sim 1.5$ mag are AGB stars with thick envelopes, post-AGB stars and young stars (Lumsden et al. 2002; Sevenster 2002). Our sample of SiO targets includes very few sources with $C-E > 1.5$.

The $K_S-[15]$ and $K_S-[12]$ are good indicators of mass-loss rate for AGB star with shells at few hundred Kelvin. All Miras have redder $K_S-[12]$ than non-Mira stars from 1.8 mag up to 6 or even 14 mag (e.g. Olivier et al. 2001; Whitelock et al. 1994). Thick-envelope OH/IR stars have typically $K_S-[15] > 4$ (Ortiz et al. 2002). The ISOGAL SiO target sample is characterised by a smaller range of ($K_S-[15]$) or (K_S-D) values than the MSX sample, as shown in Fig. 10, suggesting that the MSX sample includes a tail of sources with optically thick envelopes. However, this will be verified after correction for extinction (Paper III; Paper IV).

Figure 10 shows a strong correlation, between K_S and ($K_S-[15]$) or (K_S-D), which is due to the way we selected our original sample. In fact, due to the general correlation of SiO maser emission and infrared luminosity (Bujarrabal et al. 1987), we selected only sources with $[15] < 3.4$ in order to be able to detect the expected SiO line. The [15] and D magnitudes range from ~ 3.4 to ~ 1.0 . This narrow range generates the correlation seen in Fig. 10.

Figure 10 also shows that the two samples, ISOGAL and MSX, overlap largely, although there are some minor systematic differences. There is a vertical shift between the ISOGAL and MSX sequence, with the MSX sources brighter for a given colour. This effect is due to the different sensitivity between the MSX D band and ISOGAL surveys. MSX targets have on average a brighter D (or [15]) magnitude than the ISOGAL targets (see Fig. 9). This fact translates in differences in distance between the two samples and suggest that the MSX stars are closer on average; the two samples are also distributed differently in longitude (see Fig. 1).

On the basis of this comparison in the following we combine the results obtained with the ISOGAL sample with those obtained with the MSX sample, taking into account that there are some minor differences between the two samples.

4. Some other remarks on the SiO targets

4.1. SIMBAD search

A SIMBAD search revealed some extra information about our SiO targets.

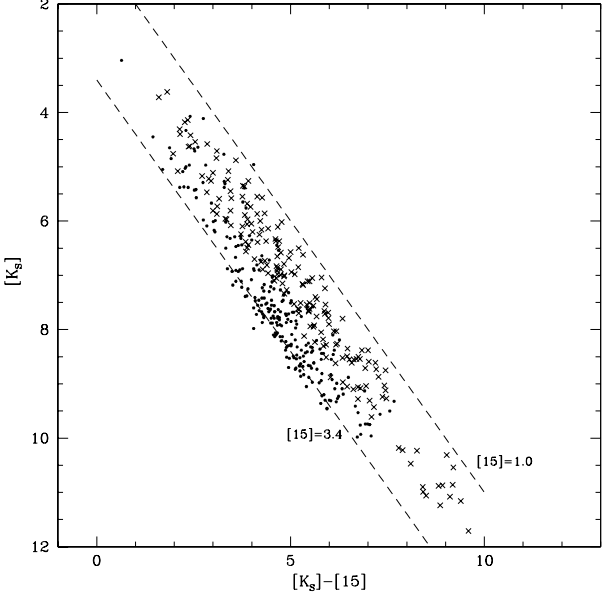


Fig. 10. 2MASS K_S versus $(K_S - [15])$ or $(K_S - D)$. Filled circles indicate objects from the ISOGAL sample, for which we plot $(K_S - [15])$; and crosses indicate objects from the MSX sample, for which we plot $(K_S - D)$. The two dashed lines correspond to $[15] = 3.4$ and 1.0 mag.

Sources #7, #286 and #303 are included in the catalogue of late-type stars in the inner Galactic region by Raharto et al. (1984) as spectral types M6, M7 and M6.5, respectively.

#153 is a well known Mira star, TLE 53, with a period of 480 d, located in Baade's window (e.g. Glass et al. 1995). Our sample also includes 15 LPVs found by Glass et al. (2001) within 0.3° from the Galactic center and 19 candidate variable stars from the list of Schultheis et al. (2000) (listed in Table 2 and 3 of Paper I).

A few sources are given in the literature as possible red supergiants or extremely luminous AGB stars: #25, #32, #92 and #295 correspond to sources #6, #8, #31 and #5 of Nagata et al. (1993), respectively; #356 is classified as bulge M supergiant by Raharto (1991) and Stephenson (1992) also lists it among distant luminous early type stars.

#127 (IRAS 17500–2512), #178 (IRAS 18040–2028), #188 (IRAS 18060–1857), #252 (IRAS 18285–1033), #265 (IRAS 18367–0507) and #434 (IRAS 18415–0355) are listed by (Kwok et al. 1997) among sources detected with the IRAS Low Resolution Spectrometer, in the range $8\text{--}23\ \mu\text{m}$ and with a resolution, $\lambda/\Delta\lambda \sim 20 - 40$. Four spectra are noisy or incomplete, while the spectra of #178 (IRAS 18040–2028), #434 (IRAS 18415–0355) are classified as featureless; they are probably evolved stars with negligible amounts of circumstellar dust. For those two objects, at longitudes 9.7 and 28.6° respectively, we also compute a moderate mass-loss rate of $5 - 7 \times 10^{-7}\ M_\odot\ \text{yr}^{-1}$ (Paper III).

#164, IRAS 17590–2412, is classified as a Li K giant star by de La Reza et al. (1997). There is a significant

difference between the SiO heliocentric velocity $V_{hel} = +4.4 \pm 1.0\ \text{km s}^{-1}$ and the optical heliocentric velocity $V_{hel} = -14.5 \pm 1.0\ \text{km s}^{-1}$ (Torres 1999, de La Reza *priv. communication*). Since the SiO maser velocity is usually coincident with the stellar velocity within few km s^{-1} (e.g. Habing 1996), we suggest that the SiO emitter is not associated with the G8II star, IRAS 17590–2412/PDS 482, which however is the only mid-infrared source within the IRAM beam and the association between the ISOGAL and DENIS source is of excellent quality (flag=5).

#189, IRAS 18059–2554, is given by Lynch & Rossano (1990) as a possible member of the globular cluster NGC6553. The stellar line-of-sight velocity, obtained through the SiO maser line, is $161.2\ \text{km s}^{-1}$. Because the cluster mean line-of-sight velocity is $7\ \text{km s}^{-1}$ with $\sigma = 14\ \text{km s}^{-1}$ (Coelho et al. 2001), we conclude that IRAS 18059–2554 is not a member of the cluster.

Twenty-eight of our 86 GHz SiO targets were previously observed for 43 GHz SiO maser emission. These are discussed in Sect. 4.5 of Paper I. For the strongest 86 GHz maser sources within 2.2° of the Galactic Centre from Paper I we recently used the Very Large Array (VLA) to observe the two 43 GHz SiO maser lines ($v=0$ and $v=1$) simultaneously (Sjouwerman et al. 2003).

We excluded from our SiO maser survey the OH/IR stars detected by Sevenster et al. (1997a,b, 2001), Sjouwerman et al. (1998) and Lindqvist et al. (1992). However, due to intrinsic source variability and the limited sensitivity of the Sevenster et al. surveys, we still included 4 OH/IR stars, as found with a SIMBAD search: #181, #226 and #257, all with detected SiO maser emission, coincide in position and velocity with OH9.84+0.01, OH17.43–0.08 and OH25.05+0.28, respectively (Blommaert et al. 1994); #409 (IRAS 18142–1600), not detected in our SiO survey, corresponds to OH #280 (OH14.805+0.150) listed by Te Lintel Hekkert et al. (1989).

4.2. Is the targeted star the actual SiO emitter?

Using the IRAM-30m telescope, we detected 86 GHz SiO maser emission toward 268 of our targeted positions, where three positions showed a double detection (#21–#22, #64–#65 and #78–#79).¹ To confirm that our targets are the actual SiO emitters, we need to examine all other possible objects falling inside the $29''$ (FWHM) IRAM beam. Due to the correlation between intensity of the maser line and mid-infrared brightness (Bujarrabal et al. 1987), we can restrict the analysis to

¹ Throughout the paper for statistic computations only one infrared source, the targeted, is considered for these three positions. A second mid-infrared source is found within the IRAM beam at the position of the SiO sources #78 and #79 (separation $\sim 12''$), and at the position of the SiO sources #21 and #22 (separation of $\sim 15''$) (see Paper I) and is given in Table 2.

only mid-infrared objects. Considering the 379 SiO targets with an MSX identification, we found in all but one case only one target inside the 86 GHz beam. Considering the 267 SiO targets with an ISOGAL identification, 89% are unique ISOGAL objects inside the main beam. SiO maser emission was detected towards 19 of our 29 positions with more than one ISOGAL source in the beam and in all cases the targeted star is the brightest 15 μm source.

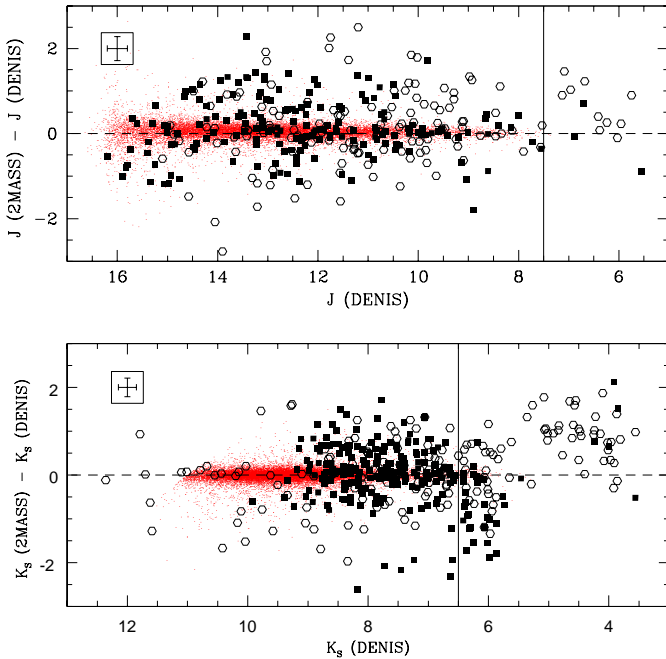


Fig. 11. Upper Panel: Difference between 2MASS and DENIS J magnitudes versus the DENIS J magnitude. Filled squares represent the ISOGAL SiO targets. For comparison small dots show ID-PSC and 2MASS associations obtained in several ISOGAL fields, which have a distribution of their J variations consistent with a gaussian distribution centred at zero. No correction for offset in the photometric zeropoint was applied. Open circles represent the MSX targets, which have indications of variability at mid-infrared wavelengths. The error bars shown within the box are $\pm 1\sigma$ mag. The vertical line indicates the DENIS saturation limit. **Lower Panel:** Comparison of the 2MASS and DENIS K_s magnitudes versus the DENIS K_s magnitude. Symbols are as in the top panel.

5. Variability

The 86 GHz SiO maser line intensity is observed to be stronger in O-rich Mira stars than in other types of AGB stars (Bujarrabal 1994; Nyman et al. 1993). To increase our chance of detecting the SiO maser emission, we tried to select strongly variable sources (Paper I, and references therein). Therefore, our selected MSX targets all have an indication of variability in the A band. Unfortunately, the ISOGAL database does not provide direct informa-

tion on variability. However, from their position in the ISOGAL/DENIS ($K_{S0} - [15]_0$ vs. $[15]_0$) diagram we were expecting that our ISOGAL SiO targets were mainly large amplitude variables (Sect. 4.2 of Paper I). For 62 ISOGAL targets out of the 191 which have an MSX counterpart, there is an indication of variability in the A band (or for 94 in at least one of the A , C , D , and E bands).

5.1. Variability information from DENIS and 2MASS data

The comparison between the near-infrared photometry obtained during the course of the DENIS survey and that of 2MASS again confirms our hypothesis for variability in the ISOGAL sample.

The J and K_s filters used by DENIS and 2MASS are similar and therefore the measurements obtained during the course of the DENIS and 2MASS surveys are directly comparable. For non variable sources, the differences between the J magnitude of DENIS and 2MASS and the K_s magnitude of DENIS and 2MASS are smaller than 0.15 mag (Delmotte et al. 2002; Schultheis & Glass 2001, and present work).

The DENIS observations were performed between 1996 and 2000, while the relevant 2MASS observations were performed between 1998 and 2000; AGB variables have periods from 50 to 1000 days, therefore the interval of time between the observations makes it possible to derive variability information.

For each of the 61 ISOGAL fields containing our SiO targets we retrieved the corresponding 2MASS sub-catalogue, and cross-correlated the ID-PSC and the 2MASS point source positions. For our ISOGAL sample the difference between the 2MASS and DENIS J and K_s magnitudes is shown as a function of the corresponding DENIS magnitude in Fig. 11. Figure 12 shows the difference between the 2MASS and DENIS J magnitudes plotted against the time between the 2MASS and DENIS observations. The distribution of the magnitude variations of the ISOGAL targets is different compared to that of random field objects. The Kolmogorov-Smirnov test gives a zero probability for the ISOGAL targets and field stars to be extracted from the same population. For 55% of our ISOGAL stars, the difference between both the 2MASS and the DENIS J and the 2MASS and the DENIS K_s magnitudes is larger than 3 times the dispersion measured in the corresponding field. Therefore, our sample contains mostly variable stars.

Due to the simultaneity of the J and K_s measurements in both the DENIS and 2MASS surveys, a correlation is expected between the variation in the J magnitude (ΔJ) and in the K_s magnitude (ΔK_s). As shown in Fig. 13 such a correlation exists. A linear least squares fit yields

$$\Delta J = 1.57(\pm 0.03) \times \Delta K_s + 0.05 \pm (0.01).$$

The relative pulsation amplitude in the K_s band is $\sim 60\%$ of the relative amplitude in J band.

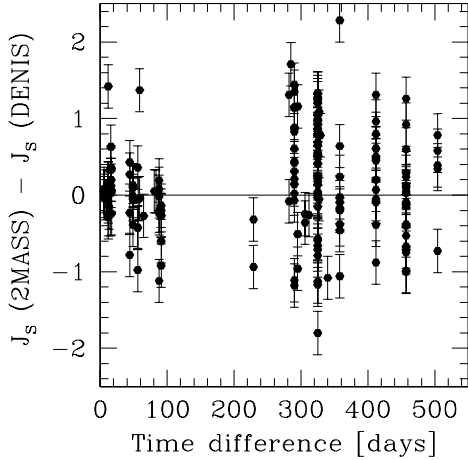


Fig. 12. The difference of the 2MASS and DENIS J magnitude versus the time between the 2MASS and DENIS observations.

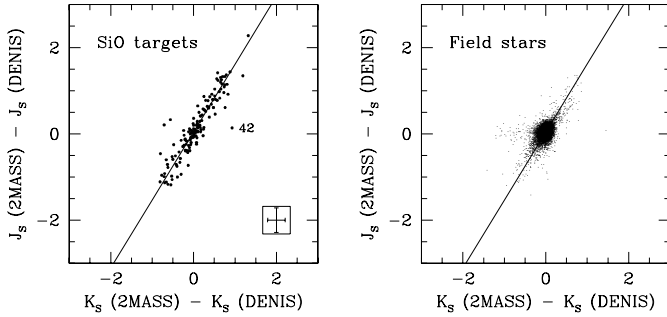


Fig. 13. Difference between the 2MASS and DENIS J magnitudes versus the difference of the 2MASS and DENIS K_s magnitudes. **Left panel:** SiO maser targets. Upper limit measurements and measurements affected by saturation are excluded. The photometry of #42 is affected by blending with another source. The continuous line shows our best fit. Within the box the typical error for sources in our range of magnitude is drawn. **Right panel:** for comparison, field stars with $J < 14$ mag.

For comparison, in Fig. 14, we also show the relation between the pulsation amplitudes in the J and K SAAO bands for two different samples of oxygen-rich stars in the solar neighbourhood (Olivier et al. 2001) and the South Galactic Cap (SGC) (Whitelock et al. 1994). The two samples have a different period distribution; most of the stars from the solar neighbourhood sample have periods between 500 and 700 d, while most of the SGC stars have periods between 150 and 450 d. Overplotting our best-fit, we see that it aligns well with the distribution of the two samples of LPVs.

A monitoring program of the near-infrared magnitudes of our SiO maser sample will provide pulsation periods and estimates of the source distances through the period-luminosity relation.

5.2. Variability flag

All the available information on variability, from MSX data (variability in at least one of the MSX band), IRAS data (variability flag > 50), DENIS-2MASS data ($\Delta J > 3\sigma(J)$ and $\Delta K > 3\sigma(K)$), or from Glass et al. (2001), from Schultheis & Glass (2001) and from Glass et al. (1995), is summarised defining a flag (var) which is 2 when variability is detected in at least one of the datasets, 1 when variability is not detected but not all the datasets were available and 0 when variability is not detected in any of the datasets. All the 188 MSX targets have the variability flag equal to 2 (due to selection). Among the 253 ISOGL targets 150 have the flag equal to 2, 81 equal to 1 and 22 equal to 0.

There is no correlation between the variability indication and the detection of SiO maser emission.

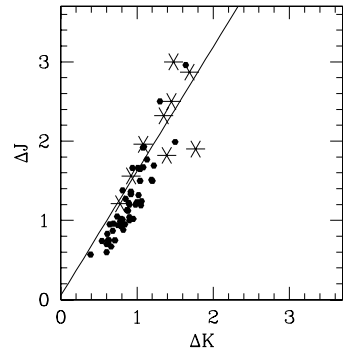


Fig. 14. Pulsation amplitude in J band versus amplitude in K band for two samples of oxygen-rich variable stars: one in the solar neighbourhood from Olivier et al. (2001) (starred points) and another in the South Galactic Cap from Whitelock et al. (1994) (filled circles). Superimposed is our best fit from Fig. 13.

6. The distribution of the SiO targets in the IRAS two-colour diagram

We cannot determine the distribution of our target sources in the two-colour IRAS diagram of van der Veen & Habing (1988) since for most of our sources we have only upper flux limits at $60\ \mu\text{m}$. Figure 15 shows the distribution of the IRAS [12] – [25] colours and recalls the regions of the IRAS two-colour diagram that separate different classes of evolved stars with circumstellar envelopes, from the bluer Mira to the thick envelope OH/IR stars. The [12] – [25] colours of our selected sources range from -1.0 to 0.4 , peaking at -0.2 , corresponding mostly to regions IIIa and VIIb. Region IIIa represents sources with moderate dust emission, being populated mostly by oxygen-rich stars with silicate emission (Kwok et al. 1997; van der Veen & Habing 1988). Region VIIb, with $60\ \mu\text{m}$ excess, contains a mixed population of early type stars with line emission and planetary nebula; however this region is scarcely populated. Considering the

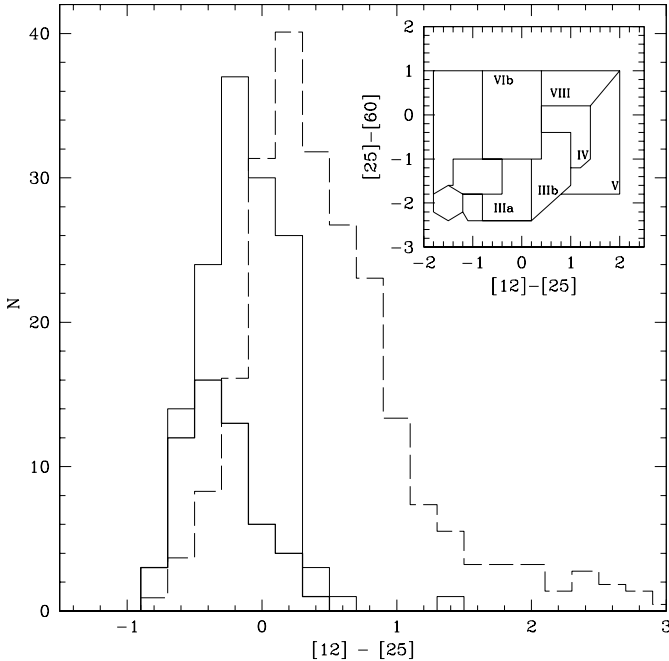


Fig. 15. Distribution of the IRAS $[12] - [25]$ colours, $-2.5 \log(F_{12}/F_{25})$. The continuous thin line indicate the distribution of our SiO targets; the thick line indicates the distribution of SiO targets with $K_S < 6.5$ mag. For comparison, the distribution of the $[12] - [25]$ colours of the OH/IR stars of Sevenster (2002) is also shown in Fig. 15. OH/IR stars are distributed over a larger and redder colour range, although partially overlapping with the colours of the SiO sample; they can have significantly (~ 1 mag) redder colours than the SiO targets. This can not be accounted for by interstellar reddening, which is only 0.1–0.2 mag for $A_V \sim 20 - 30$ mag. The stars in our sample brighter than $K_S < 6.5$ mag are bluer than those with $K_S > 6.5$ mag. They are likely to be mostly foreground stars with thinner shell, but still IRAS detectable due to their proximity.

distribution of the IRAS good quality sources, only 5% of them are located in region VIb. We conclude that our targets are mostly Mira stars with moderate mass-loss rate, in agreement with the selection criteria. For comparison, the distribution of the $[12] - [25]$ colours of the OH/IR stars of Sevenster (2002) is also shown in Fig. 15. OH/IR stars are distributed over a larger and redder colour range, although partially overlapping with the colours of the SiO sample; they can have significantly (~ 1 mag) redder colours than the SiO targets. This can not be accounted for by interstellar reddening, which is only 0.1–0.2 mag for $A_V \sim 20 - 30$ mag. The stars in our sample brighter than $K_S < 6.5$ mag are bluer than those with $K_S > 6.5$ mag. They are likely to be mostly foreground stars with thinner shell, but still IRAS detectable due to their proximity.

#177 (IRAS 18039–2052) is the only source with $[12] - [25] > 1.0$, which resembles those colours of an embedded young stellar object. However, methanol and water maser emission was unsuccessfully searched for toward this source (MacLeod et al. 1998; Molinari et al. 1996; Palla et al. 1991). Furthermore, the detection of SiO maser emission confirms that the source is a late-type star, since SiO maser emission is extremely rare in star-forming regions, with only three (extremely luminous) sources detected to date (e.g. Engels & Heske 1989; Snyder & Buhl 1974; Ukita et al. 1987). Though both the $12\mu\text{m}$ and $25\mu\text{m}$ IRAS flux densities have good quality, their association

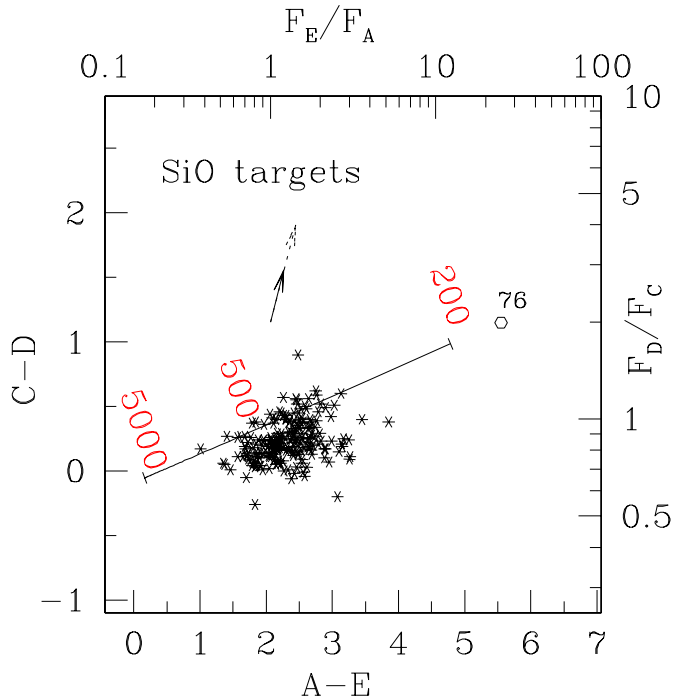


Fig. 16. MSX colour-colour plot for our SiO maser targets, similar to Fig. 5 of Lumsden et al. (2002). Stars represent AGB stars, open circles early post-AGB stars, following the classification of Sevenster (2002). Black body spectra follow the continuous line. A reddening vector for $A_V = 40$ and extinction law from Mathis (1990) is given by the solid arrow, while another one obtained using the extinction law of Lutz (1999) is represented by the dashed arrow. Note that the two vectors point in the same direction. Our SiO targets have colours similar to the objects with $9.7\mu\text{m}$ silicate emission in Kwok et al. (1997) and Lumsden et al. (2002). Object #99 is outside of the plotted region ($A - E = 3.01$ mag, $F_E/F_A = 2.4$; $C - D = -2.99$ mag, $F_D/F_C = 0.04$) (see also text).

is unreliable. In fact, the corresponding MSX source has measurements in the A , C and D bands consistent with the $12\mu\text{m}$ IRAS detection, but is not detected at $21\mu\text{m}$.

7. MSX colour-colour diagrams

Sevenster (2002) analysed the mid-infrared properties of her OH/IR sample using IRAS and MSX data. Studying a possible correspondence between regions in the two-colour IRAS diagram and the MSX $A - C$ versus $D - E$ plane she suggested that the MSX diagram can distinguish between the AGB and the post-AGB phases. The transition from a blue (< 1.8) to red (> 1.8) $A - C$ colour may correspond to a transition off the AGB to proto-planetary nebulae: the star had its last thermal pulse, and ceased to be variable. The transition from a blue (< 1.5) to a red (> 1.5) $D - E$ colour indicates a later evolutionary transition, when mass-loss starts to drop down of several order of magnitudes and there is the onset of the fast wind. Most of our SiO targets with a clear MSX counterpart

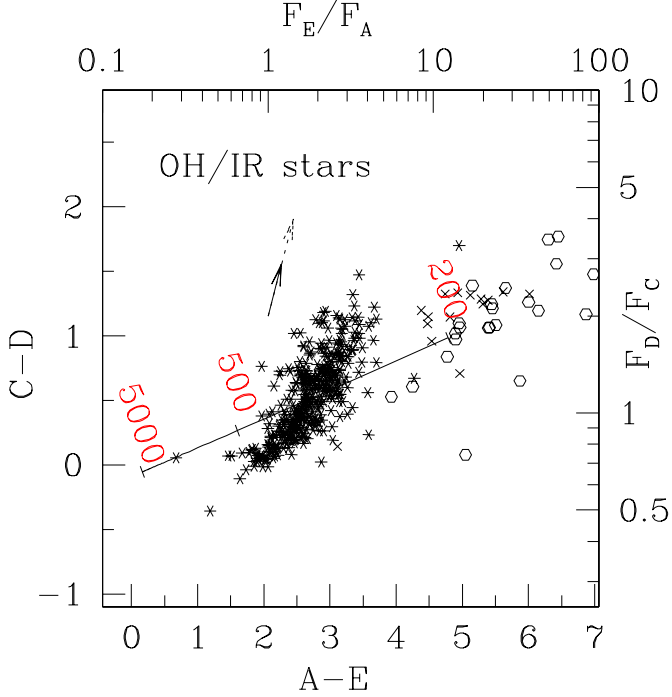


Fig. 17. MSX colour-colour plot as in Fig. 5 of Lumsden et al. (2002) for the OH/IR sample of Sevenster (2002). Symbols are as in Fig. 16, plus crosses which represent late post-AGB stars, following the classification of Sevenster (2002)

show $A - C < 1.8$ and $D - E < 1.5$, as expected for AGB stars, and comparable to the bulk of Sevenster's OH/IR sample.

According to Sevenster's criteria, only two objects, #76 and #99, which are both SiO maser emitters, are likely to be post-AGB stars. The odd colour of #99 is due to an extremely high flux density of 39 Jy measured in the C band, while the flux density in both the A and D bands is only ~ 1.7 Jy. However, the inspection of the MSX C band image does not confirm the presence of a such bright object and we conclude that the C photometry (despite its good flag) of #99 is unreliable. Source #76, LPV 12-352 (Glass et al. 2001), is located on a region of extended emission which is associated with a star forming region (Schuller 2002); this could have affected the mid-infrared colours of #76. In conclusion: the anomalous position of the sources #99 and #76 is probably due to the assignment of incorrect magnitudes.

The $A - C$ versus $D - E$ colour diagram is useful to locate post-AGB stars, which have redder colours due to their colder envelopes. However, this diagram can hardly distinguish between different thickness of the envelopes of AGB stars. Using a sample of IRAS sources with IRAS low resolution spectra (Kwok et al. 1997), Lumsden et al. (2002) showed that a different combination of MSX filters can distinguish between circumstellar envelopes with silicate feature at $9.7\ \mu\text{m}$ in emission and in absorption. Miras and OH/IR stars with the silicate feature in emission are located below the black body line in the $C - D$

versus $A - E$ diagram, while OH/IR stars with silicate feature in absorption lie above this line. In optically thick envelopes, self-absorption causes a decrease of the flux in the C and A bands, leading to an increase in $C - D$. Figure 16 shows that our SiO targets are distributed like objects with the silicate feature in emission. We note that the MSX two colour plot is not corrected for reddening. However, the reddening correction makes the sources bluer in the $C - D$ colour independently of the adopted extinction law. Furthermore, in the $C - D$ versus $A - E$ diagram the distribution of the ISOGAL and MSX samples are similar. For comparison, in Fig. 17 the MSX colour-colour plots of the Sevenster's OH/IR stars is shown, which are distributed over a wider and redder range of colours.

8. Conclusion

To increase the number of line-of-sight velocities measured toward the inner Galaxy we searched for 86 GHz SiO maser emission in a sample of 441 late-type stars. While the radio survey was described elsewhere (Messineo et al. 2002), this paper presents the infrared photometry of all our SiO targets as derived from the various accessible infrared catalogues: DENIS, 2MASS, MSX, ISOGAL and IRAS catalogues.

As described in Paper I, we initially selected the SiO targets from the ISOGAL and MSX catalogues on the basis of their near- and mid-infrared colours, and their $15\ \mu\text{m}$ magnitudes. We tried to select objects with colours typical of pulsating AGB stars with thin envelopes (Mira-like stars), while avoiding OH/IR stars and other sources with thick circumstellar envelopes.

Our analysis of the targeted stars' multi-band photometry showed that these selection criteria were quite reliable. A comparison between the DENIS and 2MASS data shows that most of them are variable stars, and moreover the correlation between the J and K_S band brightness variations is similar to that found in local dust-enshrouded Mira variable stars (Olivier et al. 2001).

The IRAS [12] – [25] colours of the SiO targets confirms that they populate mostly the region IIIa of the van der Veen and Habing classical two-colour IRAS diagram, which is a region of stars with moderate mass-loss rates and with silicate feature at $9.7\ \mu\text{m}$ in emission. The distribution of the [12] – [25] colours of the SiO targets overlaps with the distribution of the colours of OH/IR stars, which however are distributed over a larger and redder range of colours (mostly in region IIIa and IIIb). Following the work of Sevenster (2002) and Lumsden et al. (2002), those properties can be translated and seen in the MSX $C - D$ vs. $A - E$ diagram. The SiO targets have a narrower $C - D$ colour range and are located below the black-body line, differently from the thick-envelope OH/IR stars.

The two subsamples, the MSX-selected objects and the ISOGAL selected objects have very similar infrared properties but differ slightly in the average apparent magnitude, the MSX sample being on average a little brighter. This difference is, however, smaller than the spread in

magnitudes of each subsample. In forthcoming papers we usually will combine the two subsamples into one.

Acknowledgements. We are grateful to G. Simon for providing the DENIS data and to M. Sevenster for her constructive criticism. We thank F. Bertoldi, M. Johnston-Hollitt and F. Schuller for their careful reading and commenting of an earlier version of the manuscript.

We acknowledge using the cross-correlation package CataPack developed by P. Montegriffo at the Bologna Observatory.

The DENIS project is supported, in France by the Institut National des Sciences de l'Univers, the Education Ministry and the Centre National de la Recherche Scientifique, in Germany by the State of Baden-Württemberg, in Spain by the DGICYT, in Italy by the Consiglio Nazionale delle Ricerche, in Austria by the Fonds zur Förderung der wissenschaftlichen Forschung and the Bundesministerium für Wissenschaft und Forschung. The IRAS data base server of the Space Research Organisation of the Netherlands (SRON). This publication makes use of data products from the Two Micron All Sky Survey, which is a joint project of the University of Massachusetts and the Infrared Processing and Analysis Center/California Institute of Technology, funded by the National Aeronautics and Space Administration and the National Science Foundation. This research made use of data products from the Midcourse Space Experiment, the processing of which was funded by the Ballistic Missile Defence Organization with additional support from the NASA office of Space Science. This research has made use of the SIMBAD data base, operated at CDS, Strasbourg, France. The work of MM is funded by the Netherlands Research School for Astronomy (NOVA) through a *netwerk 2, Ph.D. stipend.*

References

Beichman, C. A., Chester, T. J., Skrutskie, M., Low, F. J., & Gillett, F. 1998, PASP, 110, 480

Beichman, C. A., Neugebauer, G., Habing, H. J., Clegg, P. E., & Chester, T. J. 1988, in NASA RP-1190, Vol. 1 (1988)

Blommaert, J. A. D. L., van Langevelde, H. J., & Michiels, W. F. P. 1994, A&A, 287, 479

Bujarrabal, V. 1994, A&A, 285, 953

Bujarrabal, V., Planesas, P., & del Romero, A. 1987, A&A, 175, 164

Cesarsky, C. J., Abergel, A., Agnese, P., et al. 1996, A&A, 315, L32

Coelho, P., Barbuy, B., Perrin, M.-N., et al. 2001, A&A, 376, 136

Cutri, C. M., Skrutskie, M. F., & Van Dyk, S. 2003, available on line at <http://www.ipac.caltech.edu/2mass/>

de La Reza, R., Drake, N. A., da Silva, L., Torres, C. A. O., & Martin, E. L. 1997, ApJ, 482, L77

Delmotte, N., Loup, C., Egret, D., Cioni, M.-R., & Pierfederici, F. 2002, A&A, 396, 143

Dutra, C. M., Santiago, B. X., & Bica, E. 2002, A&A, 381, 219

Egan, M. P., Price, S. D., Moshir, M. M., et al. 1999, AFRL-VS-TR-1999, 1522

Engels, D. & Heske, A. 1989, A&AS, 81, 323

Epchtein, N., de Batz, B., Copet, E., et al. 1994, Ap&SS, 217, 3

Glass, I. S., Matsumoto, S., Carter, B. S., & Sekiguchi, K. 2001, MNRAS, 321, 77

Glass, I. S., Whitelock, P. A., Catchpole, R. M., & Feast, M. W. 1995, MNRAS, 273, 383

Habing, H. J. 1996, A&A Rev., 7, 97

Kessler, M. F., Steinz, J. A., Anderegg, M. E., et al. 1996, A&A, 315, L27

Kwok, S., Volk, K., & Bidelman, W. P. 1997, ApJS, 112, 557

Lindqvist, M., Winnberg, A., Habing, H. J., & Matthews, H. E. 1992, A&AS, 92, 43

Lumsden, S. L., Hoare, M. G., Oudmaijer, R. D., & Richards, D. 2002, MNRAS, 336, 621

Lutz, D. 1999, in ESA SP-427: The Universe as Seen by ISO, Vol. 427, 623

Lynch, D. K. & Rossano, G. S. 1990, AJ, 100, 719

MacLeod, G. C., van der Walt, D. J., North, A., et al. 1998, AJ, 116, 2936

Mathis, J. S. 1990, ARA&A, 28, 37

Messineo, M., Habing, H. J., Sjouwerman, L. O., Omont, A., & Menten, K. M. 2002, A&A, 393, 115 (Paper I)

—. 2003a, A&A in preparation (Paper III)

—. 2003b, A&A in preparation (Paper IV)

Molinari, S., Brand, J., Cesaroni, R., & Palla, F. 1996, A&A, 308, 573

Nagata, T., Hyland, A. R., Straw, S. M., Sato, S., & Kawara, K. 1993, ApJ, 406, 501

Nyman, L.-A., Hall, P. J., & Le Bertre, T. 1993, A&A, 280, 551

Ojha, D. K., Omont, A., Schuller, F., et al. 2003, A&A, 403, 141

Olivier, E. A., Whitelock, P., & Marang, F. 2001, MNRAS, 326, 490

Omont, A., Gilmore, G. F., Alard, C., et al. 2003, A&A, 403, 975

Ortiz, R., Blommaert, J. A. D. L., Copet, E., et al. 2002, A&A, 388, 279

Palla, F., Brand, J., Comoretto, G., Felli, M., & Cesaroni, R. 1991, A&A, 246, 249

Price, S. D., Egan, M. P., Carey, S. J., Mizuno, D. R., & Kuchar, T. A. 2001, AJ, 121, 2819

Raharto, M. 1991, Proceedings of the Astronomical Society of Australia, 9, 306

Raharto, M., Hamajima, K., Ichikawa, T., Ishida, K., & Hidayat, B. 1984, Annals of the Tokyo Astronomical Observatory, 19, 469

Schuller, F. 2002, PhD Thesis: Université Pierre et Marie Curie, Paris 6.

Schuller, F., Ganesh, S., Messineo, M., et al. 2003, A&A, 403, 955

Schultheis, M., Ganesh, S., Glass, I. S., et al. 2000, A&A, 362, 215

Schultheis, M. & Glass, I. S. 2001, MNRAS, 327, 1193

Schultheis, M., Lançon, A., Omont, A., Schuller, F., & Ojha, D. K. 2003, A&A, 405, 531

Sevenster, M. N. 2002, AJ, 123, 2772

Sevenster, M. N., Chapman, J. M., Habing, H. J., Killeen, N. E. B., & Lindqvist, M. 1997a, A&AS, 122, 79

—. 1997b, A&AS, 124, 509

Sevenster, M. N., van Langevelde, H. J., Moody, R. A., et al. 2001, A&A, 366, 481

Simon, G. 2003, in preparation

Sjouwerman, L. O., Messineo, M., & Habing, H. J. 2003, Astron. Nachr., Vol. 324, No. S1., "The central 300 parsecs of the Milky Way"

Sjouwerman, L. O., van Langevelde, H. J., Winnberg, A., & Habing, H. J. 1998, A&AS, 128, 35

Smak, J. 1964, ApJS, 9, 141

Snyder, L. E. & Buhl, D. 1974, ApJ, 189, L31

Stanek, K. Z. 1998, Using the DIRBE/IRAS All-Sky Reddening Map to Select Low-Reddening Windows Near the Galactic Plane, preprint [astro-ph/9802307]

Stephenson, C. B. 1992, AJ, 103, 263

Te Lintel Hekkert, P., Versteege-Hensel, H. A., Habing, H. J., & Wiertz, M. 1989, A&AS, 78, 399

Torres, C. A. O. 1999, Publicação Especial do Observatorio Nacional 10

Ukita, N., Hasegawa, T., Kaifu, N., et al. 1987, in IAU Symp. 115: Star Forming Regions, 178

van der Veen, W. E. C. J. & Habing, H. J. 1988, A&A, 194, 125

Whitelock, P., Menzies, J., Feast, M., et al. 1994, MNRAS, 267, 711